



## Giant Ferroelectric Polarization of $\text{CaMn}_7\text{O}_{12}$ Induced by a Combined Effect of Dzyaloshinskii-Moriya Interaction and Exchange Striction

X. Z. Lu,<sup>1</sup> M.-H. Whangbo,<sup>2</sup> Shuai Dong,<sup>3</sup> X. G. Gong,<sup>1</sup> and H. J. Xiang<sup>1,\*</sup>

<sup>1</sup>Key Laboratory of Computational Physical Sciences (Ministry of Education), State Key Laboratory of Surface Physics, and Department of Physics, Fudan University, Shanghai 200433, P. R. China

<sup>2</sup>Department of Chemistry, North Carolina State University, Raleigh, North Carolina 27695-8204, USA

<sup>3</sup>Department of Physics, Southeast University, Nanjing 211189, P. R. China

(Received 2 February 2012; published 2 May 2012)

By extending our general spin-current model to noncentrosymmetric spin dimers and performing density functional calculations, we investigate the causes for the helical magnetic order and the origin of the giant ferroelectric polarization of  $\text{CaMn}_7\text{O}_{12}$ . The giant ferroelectric polarization is proposed to be caused by the symmetric exchange striction due to the canting of the  $\text{Mn}^{4+}$  spin arising from its strong Dzyaloshinskii-Moriya interaction. Our study suggests that  $\text{CaMn}_7\text{O}_{12}$  may exhibit a novel magneto-electric coupling mechanism in which the magnitude of the polarization is governed by the exchange striction, but the direction of the polarization by the chirality of the helical magnetic order.

DOI: 10.1103/PhysRevLett.108.187204

PACS numbers: 75.85.+t, 71.20.-b, 75.30.Et, 77.80.-e

A crucial issue to solve in the field of spintronics is how to control the magnetism of a solid effectively with an electric field. Prospective candidates that can potentially host a strong magnetoelectric (ME) effect are multiferroics in which both magnetic and ferroelectric orders can coexist to host a strong magnetoelectric (ME) effect [1,2]. In particular, those with polarizations driven by a magnetic order are promising because of their intrinsic ME coupling. A direct coupling between magnetism and ferroelectricity was demonstrated in several multiferroics [3–8], but the magnitudes of their polarizations are usually rather small. Very recently, it was reported [9,10] that a mixed-valent manganate  $\text{CaMn}_7\text{O}_{12}$ , consisting of one  $\text{Mn}^{4+}$  and six  $\text{Mn}^{3+}$  ions per formula unit (FU), exhibits a giant ferroelectric polarization ( $2870 \mu\text{C}/\text{m}^2$ ) along the  $c$  direction at 90 K, below which it adopts a helical magnetic order with propagation vector  $(0, 1, 0.963)$ . This giant ferroelectric polarization in  $\text{CaMn}_7\text{O}_{12}$  is puzzling: according to the spin-current model of Katsura *et al.* [11], the helical magnetic structure cannot induce a nonzero ferroelectric polarization. Recently, we presented a more general model [12] that explains the ferroelectric polarizations induced by a helical magnetic structure. These ferroelectric polarizations arise from spin-orbit coupling (SOC) and hence are very weak in general. Currently, the microscopic origin of the giant ferroelectric polarization in  $\text{CaMn}_7\text{O}_{12}$  is unknown, although a phenomenological ferroaxial coupling mechanism [10,13] has been proposed.

In this Letter, we show on the basis of first principles density functional theory (DFT) calculations that the giant ferroelectric polarization originates mainly from the symmetric exchange striction associated with a particular spin exchange path between  $\text{Mn}^{4+}$  and  $\text{Mn}^{3+}$  ions, the Dzyaloshinskii-Moriya (DM) antisymmetric interaction [14] between them is unusually strong for magnetic

insulators (i.e.,  $|D/J| \approx 0.54$  compared with  $|D/J| \leq \sim 0.1$  usually expected [14]), and  $\text{CaMn}_7\text{O}_{12}$  exemplifies a novel ME coupling mechanism.

Above  $\sim 440$  K  $\text{CaMn}_7\text{O}_{12}$  has a distorted perovskite structure in which, per FU, one  $\text{Ca}^{2+}$  and three  $\text{Mn}^{3+}$  ( $\text{Mn1}$ ) ions occupy the  $A$  sites with the remaining four  $\text{Mn}^{3.25+}$  ions at the  $B$  sites. On cooling below  $\sim 440$  K  $\text{CaMn}_7\text{O}_{12}$  undergoes a structural phase transition adopting the space group  $R\bar{3}$  [15], in which the four  $\text{Mn}^{3.25+}$  ions per FU undergo a charge order into one  $\text{Mn}^{4+}$  ( $\text{Mn3}$ ) and three  $\text{Mn}^{3+}$  ( $\text{Mn2}$ ) ions without breaking the inversion symmetry. The  $\text{Mn1}^{3+}$  and  $\text{Mn2}^{3+}$  ions form chains along the  $c$  direction (hereafter  $//c$ -chains) [Fig. 1(a)] such that, in every three adjacent  $//c$ -chains, the interchain  $\text{Mn1-Mn2}$  connections form a spiral chain [Figs. 1(a) and 1(b)]. The spiral chains of  $\text{Mn}^{3+}$  ions share their  $//c$ -chains to form hexagonal tunnels [Fig. 1(c)], which are each occupied by a chain of alternating  $\text{Mn}^{4+}$  and  $\text{Ca}^{2+}$  ions so that the  $\text{Mn}^{4+}$  and  $\text{Ca}^{2+}$  ions are each surrounded by six  $//c$ -chains of  $\text{Mn}^{3+}$  ions [Fig. 1(d)]. The neutron diffraction measurements [10] show that in the helical magnetic state in the temperature range  $T_{N2}(48 \text{ K}) < T < T_{N1}(90 \text{ K})$ , the  $\text{Mn}^{3+}$  spins of each  $//c$ -chain are nearly perpendicular to the  $c$ -axis and are ferromagnetic (FM) [Fig. 1(e)]. In each spiral chain made up of three  $//c$ -chains, the spins of the three FM chains have a compromised arrangement with  $120^\circ$  between the spins of adjacent  $//c$ -chains [Fig. 1(f)], showing the presence of spin frustration between them. The  $\text{Mn}^{4+}$  spins, which are nearly perpendicular to the  $c$ -axis, make an angle of  $\sim 90^\circ$  with the  $\text{Mn}^{3+}$  spins in one set of the three FM chains [dotted triangle in Fig. 1(f)] and  $\sim 30^\circ$  with the  $\text{Mn}^{3+}$  spins in another set of the three FM chains [dashed triangle in Fig. 1(f)] [hereafter, the  $(90^\circ, 30^\circ)$  spin arrangement].

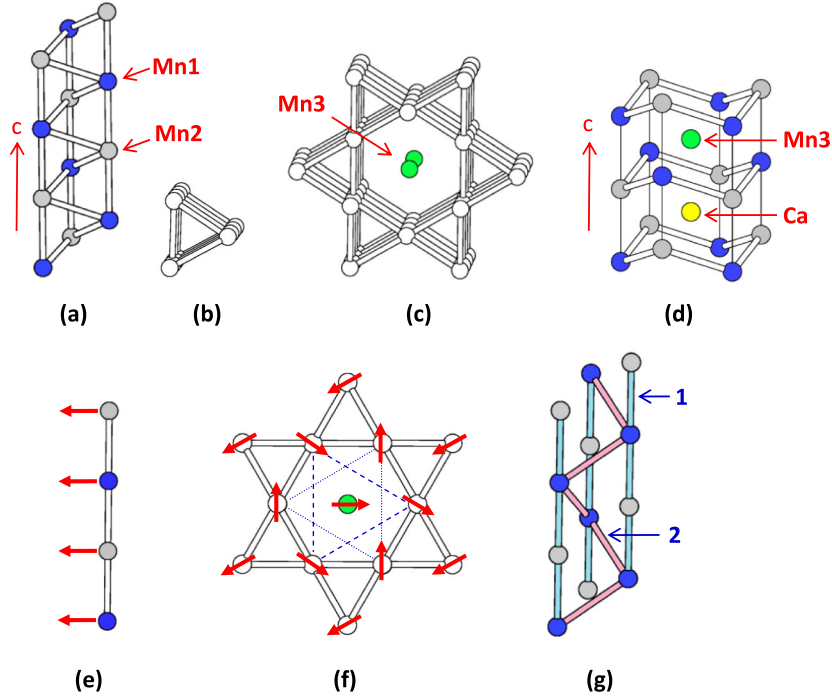


FIG. 1 (color online). (a) Three adjacent  $//c$  chains of  $\text{Mn}^{3+}$  ions, where the blue and grey circles represent the  $\text{Mn1}$  and  $\text{Mn2}$  atoms, respectively. (b) A spiral chain made up of three adjacent  $//c$ -chains of  $\text{Mn}^{3+}$  ions viewed approximately along the  $c$  direction. (c) Three-dimensional arrangement of the  $\text{Mn}^{3+}$  and  $\text{Mn}^{4+}$  ions in  $\text{CaMn}_7\text{O}_{12}$  viewed approximately along the  $c$  direction. For simplicity, the  $\text{Ca}^{2+}$  ions are not shown. (d) Arrangements of the  $\text{Mn}^{3+}$  ions surrounding two adjacent  $\text{Mn}^{4+}$  and  $\text{Ca}^{2+}$  ions, where green and yellow circles represent the  $\text{Mn}^{3+}$  and  $\text{Ca}^{2+}$  ions, respectively, and the blue and grey circles the  $\text{Mn1}^{3+}$  and  $\text{Mn2}^{3+}$  ions, respectively. (e) Arrangement of the  $\text{Mn}^{3+}$  spins in a single  $//c$  chain. (f) Projection view of the  $\text{Mn}^{3+}$  and  $\text{Mn}^{4+}$  spin arrangements in  $\text{CaMn}_7\text{O}_{12}$  along the  $c$  direction, where each triangle represents three  $//c$ -chains forming a spiral chain. The spins of each FM  $//c$ -chain are represented by a single spin. (g) Two important spin exchange paths in a spiral chain made up of three adjacent  $//c$ -chains, where the numbers 1 and 2 refer to  $J_1$  and  $J_2$ , respectively.  $J_1$  is FM, and  $J_2$  is AFM.

To account for the observed magnetic structure of  $\text{CaMn}_7\text{O}_{12}$  below 90 K, we first evaluate various symmetric spin exchange interactions between the  $\text{Mn1}^{3+}$ ,  $\text{Mn2}^{3+}$  and  $\text{Mn3}^{4+}$  ions. These ions form the  $\text{Mn1O}_4$  square planes, the axially compressed  $\text{Mn2O}_6$  octahedra, and the  $\text{Mn3O}_6$  octahedra [Figs. 2(a)–2(c)], so that their  $d$ -states are split as depicted in Fig. 2(d) according to the computed partial density of states (see Part 3 of [16]). If the distance between the magnetic ions in a spin dimer is restricted to be shorter than 3.7 Å, there are seven different spin exchange paths  $J_1$ – $J_7$  between the  $\text{Mn1}^{3+}$ ,  $\text{Mn2}^{3+}$  and  $\text{Mn3}^{4+}$  ions (see Fig. S1 of [16]). We evaluate the values of the spin exchanges  $J_1$ – $J_7$  by performing the energy-mapping analysis [17] on the basis of DFT +  $U$  calculations (see Part 1 of [16]). The justification for the use of  $U = 2$  and 3 eV in our calculations are given in Part 8 of [16]. Unless mentioned otherwise, results from our calculations with  $U = 3$  eV are presented in the following. The exchange  $J_1$  between adjacent  $\text{Mn1}^{3+}$  and  $\text{Mn2}^{3+}$  ions in a  $//c$ -chain [Fig. 2(a)] is strongly FM ( $J_1 = -5.57$  meV, which is an effective spin exchange obtained by setting  $|\mathbf{S}_i| = 1$ , namely,  $J_{ij}^{\text{eff}} = J_{ij}S_iS_j$  for a spin dimer  $ij$ ). The hybridization between the occupied  $t_{2g}$  states of one Mn ion and the empty

$e_g$  states of the neighboring Mn ion is stronger for the FM than for the AFM spin arrangement because the energy difference between the occupied and empty  $d$  states is smaller for the FM arrangement, thereby leading to FM  $J_1$ , which is responsible for the FM arrangement of the  $\text{Mn}^{3+}$  spins in each  $//c$ -chain. The exchange  $J_2$  between  $\text{Mn1}^{3+}$  spins between adjacent  $//c$ -chains [Fig. 2(b)] is strongly AFM ( $J_2 = 6.37$  meV) due to the Mn-O...O-Mn supersuperexchange interactions [18]. Consequently, these interchain AFM exchanges cause a strong spin frustration between adjacent FM  $//c$ -chains [Fig. 1(g)], and hence the three FM  $//c$ -chains in each spiral chain adopt the compromised  $120^\circ$  spin arrangement [Fig. 1(f)].

Our DFT +  $U$  + SOC calculations show that the  $\text{Mn1}^{3+}$  has an easy-axis anisotropy (1.0 meV/Mn) with the easy-axis perpendicular to the  $\text{Mn1O}_4$  plane [Fig. 2(a)], while the  $\text{Mn2}^{3+}$  ion has an easy-plane anisotropy (1.5 meV/Mn) with the easy-plane perpendicular to the axially-compressed Mn-O bonds (see Part 4 of [16] for details). As depicted in Fig. 2(a), the easy-axis of the  $\text{Mn1}^{3+}$  spin and the easy-plane of the  $\text{Mn2}^{3+}$  spin are much closer to the  $ab$ -plane than to the  $c$ -axis. The observed orientation of the  $\text{Mn1}^{3+}$  and  $\text{Mn2}^{3+}$  spins [Fig. 1(e)] [10],

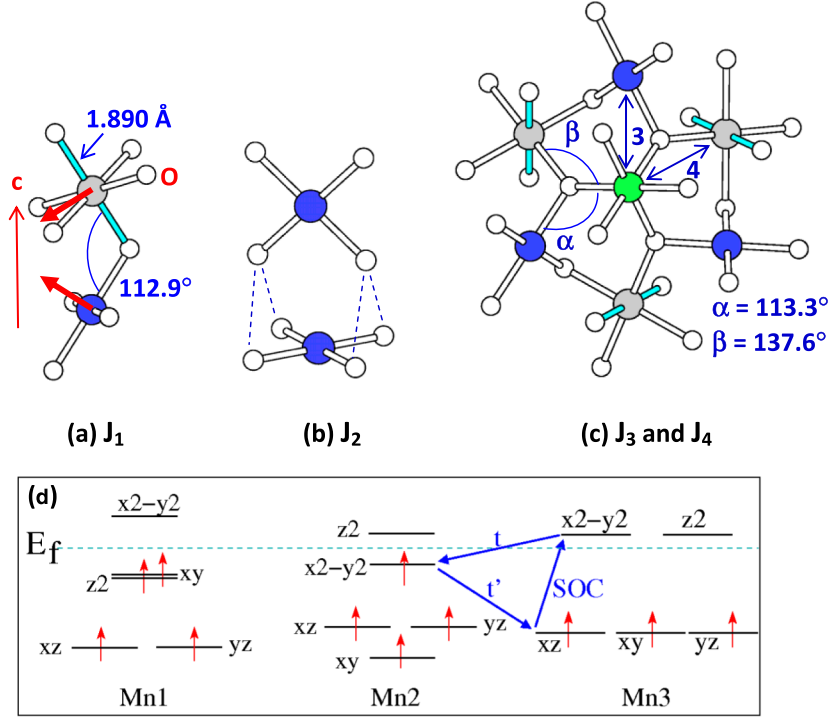


FIG. 2 (color online). (a) The spin exchange path  $J_1$  between adjacent  $\text{Mn}1^{3+}$  (blue circle) and  $\text{Mn}2^{3+}$  (grey circle) ions in each  $//c$ -chain. (b) The spin exchange path  $J_2$  between  $\text{Mn}1^{3+}$  ions that occurs between adjacent  $//c$ -chains, where the dotted lines are the  $\text{O} \dots \text{O}$  contacts shorter than the van der Waals radii sum  $3.04 \text{ \AA}$  (namely,  $2.708, 2.727, 2.763,$  and  $2.831 \text{ \AA}$ ). (c) The exchange path  $J_3$  between  $\text{Mn}1^{3+}$  (blue circle) and  $\text{Mn}3^{4+}$  (green circle), and the exchange path  $J_4$  between  $\text{Mn}2^{3+}$  (grey circle) and  $\text{Mn}3^{4+}$ . (d) The  $d$ -state split patterns of the  $\text{Mn}1\text{O}_4$  square plane, the axially compressed  $\text{Mn}2\text{O}_6$  octahedron, and the  $\text{Mn}3\text{O}_6$  octahedron that best describe the partial density of states [16]. The blue arrows indicate the  $d$ -states of  $\text{Mn}3^{4+}$  and  $\text{Mn}2^{3+}$  ions involved in the three hopping processes leading to the large DM interaction between adjacent  $\text{Mn}3^{4+}$  and  $\text{Mn}2^{3+}$  ions in the spin exchange path  $J_4$ .

in which all spins are almost perpendicular to the  $c$ -axis, is a combined effect of the single-ion anisotropies and the strong FM spin exchange  $J_1$  between adjacent  $\text{Mn}1^{3+}$  and  $\text{Mn}2^{3+}$  ions.

Let us now consider the preferred orientation of the  $\text{Mn}3^{4+}$  spin. Each  $\text{Mn}3^{4+}$  ion is surrounded by six  $\text{Mn}1^{3+}$  ions and also by six  $\text{Mn}2^{3+}$  ions [Figs. 1(d), 3(a), and 3(b)]. Thus, each  $\text{Mn}3^{4+}$  ion has six spin exchanges  $J_3$  with the  $\text{Mn}1^{3+}$  ions and six spin exchanges  $J_4$  with the  $\text{Mn}2^{3+}$  ions [Figs. 1(d) and 2(c)]. Note from Figs. 1(d)–1(f) that the  $\text{Mn}1^{3+}$  and  $\text{Mn}2^{3+}$  ions have an identical spin direction if their  $c$ -axis heights are the same. In Figs. 3(a) and 3(b) depicting the environment of a  $\text{Mn}^{4+}$  surrounded by 12  $\text{Mn}^{3+}$  ions, the site number 0 refers to the  $\text{Mn}^{4+}$  ion, the site numbers 1–3 to three pairs of  $\text{Mn}1^{3+}$  and  $\text{Mn}2^{3+}$  ions with identical spin direction, and the site numbers 4–6 to another three pairs of  $\text{Mn}1^{3+}$  and  $\text{Mn}2^{3+}$  ions with identical spin direction. For simplicity, we set  $|\mathbf{S}_i| = 1$ , and define the unit vector  $\mathbf{e}_x$  along the direction of  $\mathbf{S}_1 + \mathbf{S}_4$ , and  $\mathbf{e}_y$  orthogonal to  $\mathbf{e}_x$  in the plane as in Fig. 3(a) so that  $\mathbf{e}_z = \mathbf{e}_x \times \mathbf{e}_y$  points toward the reader. Thus, if  $\mathbf{S}_1 \times \mathbf{S}_4$  is along  $\mathbf{e}_z$ , then  $\mathbf{S}_4 - \mathbf{S}_1$  is along  $\mathbf{e}_y$ , i.e.,  $\frac{\mathbf{S}_1 - \mathbf{S}_4}{|\mathbf{S}_1 - \mathbf{S}_4|} = \mathbf{e}_y \text{sign}[\mathbf{e}_z \cdot (\mathbf{S}_4 \times \mathbf{S}_1)]$ . The spins of the two different sets make the angle of  $120^\circ$  between them. Given  $\alpha$  as the angle the spin

vector  $\mathbf{S}_0$  makes with  $\mathbf{e}_x$ , then the total spin exchange interaction energy  $E_{SE}$  of a  $\text{Mn}^{4+}$  spin with its 12 adjacent  $\text{Mn}^{3+}$  spins is given by

$$\begin{aligned} E_{SE} &= (J_3 + J_4)\mathbf{S}_0 \cdot (\mathbf{S}_1 + \mathbf{S}_2 + \mathbf{S}_3 + \mathbf{S}_4 + \mathbf{S}_5 + \mathbf{S}_6) \\ &= 3(J_3 + J_4)\cos\alpha. \end{aligned} \quad (1)$$

Therefore, as long as the sum  $(J_3 + J_4)$  is negative (i.e., net FM), which is indeed the case (see Part 8 of [16]), the lowest energy occurs for  $\alpha = 0^\circ$ , i.e., for the  $(60^\circ, 60^\circ)$  arrangement of the  $\text{Mn}3^{4+}$  spins. This argument is confirmed by direct DFT +  $U$  calculations for the energy  $E_{SE}(\alpha)$  of  $\text{CaMn}_7\text{O}_{12}$  with the  $\text{Mn}1^{3+}$  and  $\text{Mn}2^{3+}$  spins fixed at the experimentally observed orientations but the spin orientation of the  $\text{Mn}3^{4+}$  ions varied as a function of the angle  $\alpha$ . We find the minimum of  $E_{SE}(\alpha)$  at  $\alpha = 0^\circ$  [Fig. 3(c)], consistent with the above analysis, but in disagreement with the experimental finding that the minimum of  $E_{SE}(\alpha)$  occurs at  $|\alpha| \approx 30^\circ$  [i.e., for the  $(90^\circ, 30^\circ)$  arrangement] [10]. DFT +  $U$  + SOC calculations show the energy minimum of  $E_{SE}(\alpha)$ —at  $\alpha_m = -11^\circ$  [Fig. 3(c)]—in qualitative agreement with experiment indicating the DM interactions to be responsible for the  $(90^\circ, 30^\circ)$  spin arrangement of the  $\text{Mn}3^{4+}$  ions (see below). We point out that  $\alpha_m = -28^\circ$  is obtained from DFT +  $U$  + SOC calculations with

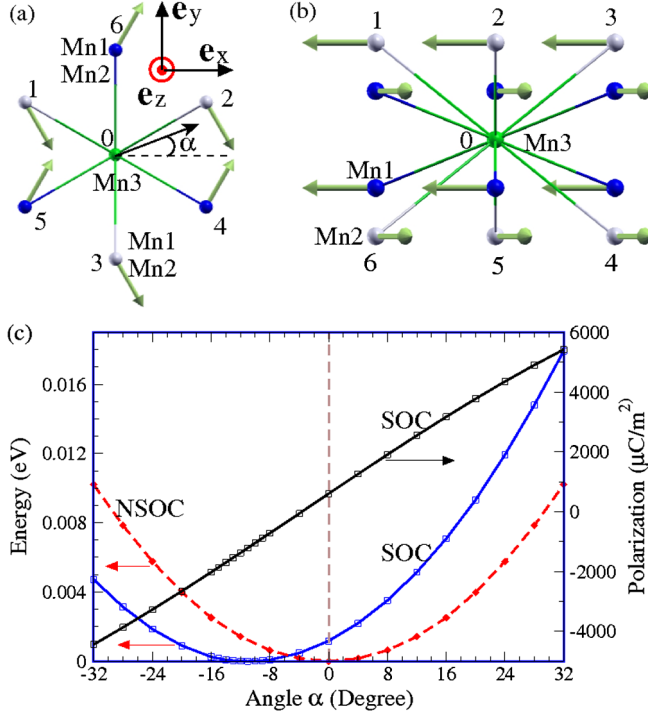


FIG. 3 (color online). (a, b) The top and side views of six  $\text{Mn1}^{3+}$  and six  $\text{Mn2}^{3+}$  ions surrounding a  $\text{Mn3}^{4+}$  ion. The directions of the  $\text{Mn1}^{3+}$  and  $\text{Mn2}^{3+}$  spins, observed experimentally, are also shown. (c) The total energy and electric polarization as a function of the  $\text{Mn3}^{4+}$  spin direction  $\alpha$  (see the text for the definition). In the absence of SOC (designated as NSOC), the energy minimum occurs when  $\alpha = 0^\circ$ . In the case of SOC,  $\alpha = -11^\circ$ .

$U = 2$  eV, in good agreement with experiment (see Part 8 of [16]).

We now examine the ferroelectric polarization of  $\text{CaMn}_7\text{O}_{12}$  by simulating the experimental helical magnetic state with the commensurate helical state  $\mathbf{k} = (0, 1, 1)$  in terms of the hexagonal unit cell. Our DFT +  $U$  + SOC calculations show that this helical state has a band gap of 0.45 eV and is more stable than the FM state by 18 meV per FU. The ferroelectric polarization of this helical state with  $|\alpha| \approx 30^\circ$  is along the  $z$  direction (i.e.,  $c$ -direction) with  $P_z = 4496 \mu\text{C}/\text{m}^2$  from DFT +  $U$  + SOC calculations, but  $P_z = 3976 \mu\text{C}/\text{m}^2$  from DFT +  $U$  calculations. Consequently, the giant ferroelectric polarization of  $\text{CaMn}_7\text{O}_{12}$  is caused mainly by exchange striction rather than by SOC.

Given the above finding, it is important to probe which symmetric spin exchange interaction is crucial for the large ferroelectric polarization. Thus we first extend our general spin current model for ferroelectric polarization [12] to include spin dimers with no centrosymmetric symmetry because the spin dimers of  $\text{CaMn}_7\text{O}_{12}$  are noncentrosymmetric (see Part 5 of [16]). For a spin dimer containing two spin sites 1 and 2 with no inversion symmetry at the center, the polarization  $\mathbf{P}_{12}$  induced by the spin arrangement  $(\mathbf{S}_1, \mathbf{S}_2)$  in the absence of SOC effect can be written

as the usual symmetric exchange striction term  $\mathbf{P}_{12}(\mathbf{S}_1, \mathbf{S}_2) = \mathbf{P}_{\text{es}}(\mathbf{S}_1 \cdot \mathbf{S}_2)$ . For the seven exchange paths of the experimental  $\text{CaMn}_7\text{O}_{12}$  structure, we evaluate their  $P_{\text{es}}$  by performing DFT +  $U$  calculations using an energy-mapping method similar to that used to extract the spin exchange parameters [17]. Our calculations show that two exchange paths  $J_4$  and  $J_5$  have the largest coefficients, namely,  $\mathbf{P}_{\text{es}}^4 = (-0.024, -0.042, 0.029) e\text{\AA}$  and  $\mathbf{P}_{\text{es}}^5 = (-0.026, -0.048, 0.054) e\text{\AA}$ . The remaining spin exchange paths lead to much smaller coefficients. The contribution of  $\mathbf{P}_{\text{es}}^5$  to the total electric polarization vanishes by symmetry, but  $\mathbf{P}_{\text{es}}^4$  has a large contribution to the total electric polarization. The large  $\mathbf{P}_{\text{es}}^4$  arises not only from the small energy gap between the occupied  $\text{Mn2}^{3+} d_{x^2-y^2} \uparrow$  state and the empty  $\text{Mn3}^{4+} e_g$  states in the FM arrangement of the spins in the  $J_4$  path but also from the large  $\angle \text{Mn3-O-Mn2}$  angle ( $137.6^\circ$ ), because both reinforce the interaction between the occupied and empty states [Fig. S5(a) and (b) of [16]]. Note from Fig. 1(f) that in the  $(90^\circ, 30^\circ)$  spin arrangement the  $\text{Mn3}^{4+}$  spins give rise to FM-like ( $\sim 30^\circ$ ) interactions with the  $\text{Mn2}^{3+}$  spins of the dashed triangle. The difference electron density map between the FM and AFM coupling cases (Fig. S5(d) of [16]) shows the transfer of some electrons from the  $\text{Mn2} d_{x^2-y^2}$  to the  $\text{Mn3} d_{z^2}$  state.

To understand the role played by SOC [19] on the spin direction of  $\text{Mn3}^{4+}$ , we calculate the DM vectors associated with the seven spin exchange paths  $J_1$ – $J_7$  using our energy-mapping method [17]. The DM vector for the  $\text{Mn2}^{3+}$  and  $\text{Mn3}^{4+}$  ions in the exchange path  $J_4$  is anomalously large, namely,  $|\mathbf{D}_4| = 1.61$  meV and  $D_4^z = 1.36$  meV. The latter is about 54% of the symmetric exchange interaction  $J_4$  (see Table S1 of [16]). Why the DM interaction  $D_4$  is so strong is discussed in Part 7 of [16]. The DM vector for the  $\text{Mn2}^{3+}$  ions in the exchange path  $J_5$  is also relatively large but is not relevant for determining the  $\text{Mn3}^{4+}$  spin direction. To see if the DM interaction associated with  $\mathbf{D}_4$  is indeed responsible for the  $\text{Mn3}^{4+}$  spin direction, we now write the total spin interaction energy  $E_{\text{tot}}$  of  $\text{Mn3}^{4+}$  with its 12 neighboring  $\text{Mn}^{3+}$  ions as  $E_{\text{tot}} = E_{\text{SE}} + E_{\text{DM}}$ , where  $E_{\text{SE}}$  is given by Eq. (1), and the DM interaction energy  $E_{\text{DM}}(\alpha)$  by

$$E_{\text{DM}}(\alpha) = \mathbf{D}_{01} \cdot [\mathbf{S}_0 \times (\mathbf{S}_1 + \mathbf{S}_4)] + \mathbf{D}_{02} \cdot [\mathbf{S}_0 \times (\mathbf{S}_2 + \mathbf{S}_5)] \\ + \mathbf{D}_{03} \cdot [\mathbf{S}_0 \times (\mathbf{S}_3 + \mathbf{S}_6)] = 3D_4^z \sin \alpha. \quad (2)$$

In deriving the above expression, use was made of the fact that  $\mathbf{D}_{01} = \mathbf{D}_{04}$  because the spin dimers 0-1 and 0-4 are related by the inversion symmetry, and  $D_{01}^z = D_{02}^z = D_{03}^z$  due to the threefold rotational symmetry. Therefore,

$$E_{\text{tot}}(\alpha) = 3(J_3 + J_4) \cos \alpha + 3D_4^z \sin \alpha \quad (3)$$

so the minimum of  $E_{\text{tot}}(\alpha)$  is obtained when the  $\text{Mn3}^{4+}$  spin is along the direction given by  $\alpha_m = \arctan[D_4^z / (J_3 + J_4)]$ . Our calculations show  $D_4^z = 1.36$  meV,

$J_3 = -3.92$  meV,  $J_4 = -2.96$  meV so that  $\alpha_m = -11.2^\circ$ , which agrees with the result from the direct first principles calculations [With the  $J_3$ ,  $J_4$  and  $D_4^z$  parameters determined from DFT +  $U$  + SOC calculations with  $U = 2$  eV, we obtain  $\alpha_m = -36^\circ$  in closer agreement with  $-28^\circ$  from the direct DFT calculations (see Part 8 of [16]). With the definition of the local coordinate system,  $\alpha_m$  does not depend on the chirality and the propagation vector of the helical state.

It should be noted that the spin orientation of  $\text{Mn}^{3+}$  is also responsible for the strong ferroelectric polarization arising from the exchange striction. Because of the three-fold rotational symmetry, the total polarization is along  $z$ . The polarization per  $\text{Mn}^{3+}$  from the exchange striction mechanism can be expressed as

$$\begin{aligned} P_z &= P_{\text{es},4}^z [\mathbf{S}_0 \cdot (\mathbf{S}_1 - \mathbf{S}_4 + \mathbf{S}_2 - \mathbf{S}_5 + \mathbf{S}_3 - \mathbf{S}_6)] \\ &= 3P_{\text{es},4}^z \mathbf{S}_0 \cdot (\mathbf{S}_1 - \mathbf{S}_4) \\ &= 3P_{\text{es},4}^z |\mathbf{S}_4 - \mathbf{S}_1| [(\cos\alpha)\mathbf{e}_x \\ &\quad + (\sin\alpha)\mathbf{e}_y] \cdot \mathbf{e}_y \text{sign}[\mathbf{e}_z \cdot (\mathbf{S}_4 \times \mathbf{S}_1)] \\ &= 3\sqrt{3}P_{\text{es},4}^z (\sin\alpha) \text{sign}[\mathbf{e}_z \cdot (\mathbf{S}_4 \times \mathbf{S}_1)]. \end{aligned} \quad (4)$$

Thus the magnitude of  $P_z$  depends almost linearly on  $\alpha$ , because  $\sin\alpha \approx \alpha$  for small  $\alpha$ . This finding is consistent with the direct DFT calculations [Fig. 3(c)]. When  $\alpha = -30^\circ$ , the polarization becomes  $-4000 \mu\text{C}/\text{m}^2$ . Thus, the large electric polarization originates from the combined effect of the exchange striction and DM interaction.

It is important to note from Eq. (4) that the direction of the polarization depends on the scalar chirality  $\sigma \propto \mathbf{e}_z \cdot (\mathbf{S}_4 \times \mathbf{S}_1) \propto \mathbf{r}_{41} \cdot (\mathbf{S}_4 \times \mathbf{S}_1)$ . Because of the presence of the DM interaction, two equivalent states with opposite electric polarizations must have the opposite spin chirality. Thus, the polarization reversal, induced by switching the electric field direction, will cause the chirality reversal of the helical spiral. This usually occurs in a multiferroic system such as  $\text{LiCu}_2\text{O}_2$  [20] where the ferroelectricity is due purely to the SOC effect. In the case of  $\text{CaMn}_7\text{O}_{12}$ , however, the mechanism of switching the spin chirality is different: The magnitude of the ferroelectric polarization in  $\text{CaMn}_7\text{O}_{12}$  is determined by the exchange striction (thus could be large), but the sign of the polarization by that of the chirality  $\sigma$  of the helical magnetic structure due to the strong DM interaction. In the ferroaxial mechanism of Johnson *et al.* [10,13], both the magnitude and the sign of the polarization are determined by the chirality  $\sigma$  of the helical magnetic structure.

Work at Fudan was partially supported by NSFC, Pujiang plan, the Special Funds for Major State Basic Research, Foundation for the Author of National Excellent Doctoral Dissertation of China, Research Program of Shanghai municipality and MOE. S. D. was supported by NSFC (Grant No. 11004027) and 973 Projects of China (Grant No. 2011CB922101).

\*hxiang@fudan.edu.cn

- [1] S.-W. Cheong and M. Mostovoy, *Nature Mater.* **6**, 13 (2007); R. Ramesh and N. A. Spaldin, *Nature Mater.* **6**, 21 (2007); S. Picozzi and C. Ederer, *J. Phys. Condens. Matter* **21**, 303201 (2009); D. Khomskii, *Physics* **2**, 20 (2009).
- [2] K. F. Wang, J.-M. Liu, and Z. F. Ren, *Adv. Phys.* **58**, 321 (2009).
- [3] T. Kimura *et al.*, *Nature (London)* **426**, 55 (2003).
- [4] A. Malashevich and D. Vanderbilt, *Phys. Rev. Lett.* **101**, 037210 (2008).
- [5] H. J. Xiang, S.-H. Wei, M.-H. Whangbo, and J. L. F. Da Silva, *Phys. Rev. Lett.* **101**, 037209 (2008).
- [6] N. Hur *et al.*, *Nature (London)* **429**, 392 (2004).
- [7] C. J. Wang, G.-C. Guo, and L. X. He, *Phys. Rev. Lett.* **99**, 177202 (2007).
- [8] K. Taniguchi, N. Abe, T. Takenobu, Y. Iwasa, and T. Arima, *Phys. Rev. Lett.* **97**, 097203 (2006).
- [9] G. Q. Zhang *et al.*, *Phys. Rev. B* **84**, 174413 (2011).
- [10] R. D. Johnson, L. C. Chapon, D. D. Khalyavin, P. Manuel, P. G. Radaelli, and C. Martin, *Phys. Rev. Lett.* **108**, 067201 (2012).
- [11] H. Katsura, N. Nagaosa, and A. V. Balatsky, *Phys. Rev. Lett.* **95**, 057205 (2005); I. A. Sergienko and E. Dagotto, *Phys. Rev. B* **73**, 094434 (2006); M. Mostovoy, *Phys. Rev. Lett.* **96**, 067601 (2006).
- [12] H. J. Xiang, E. J. Kan, Y. Zhang, M.-H. Whangbo, and X. G. Gong, *Phys. Rev. Lett.* **107**, 157202 (2011).
- [13] R. D. Johnson *et al.*, *Phys. Rev. Lett.* **107**, 137205 (2011).
- [14] T. Moriya, *Phys. Rev.* **120**, 91 (1960); *Phys. Rev. Lett.* **4**, 228 (1960).
- [15] B. Bochu *et al.*, *Solid State Commun.* **36**, 133 (1980).
- [16] See supplemental material at <http://link.aps.org/supplemental/10.1103/PhysRevLett.108.187204>.
- [17] H. J. Xiang, E. J. Kan, S.-H. Wei, M.-H. Whangbo, and X. G. Gong, *Phys. Rev. B* **84**, 224429 (2011).
- [18] M.-H. Whangbo, H.-J. Koo, and D. Dai, *J. Solid State Chem.* **176**, 417 (2003).
- [19] D. Dai, H. J. Xiang, and M.-H. Whangbo, *J. Comput. Chem.* **29**, 2187 (2008).
- [20] S. Seki *et al.*, *Phys. Rev. Lett.* **100**, 127201 (2008).